

CoIr-carbon complexes with magnetic anisotropies larger than 0.2 eV: a density-functional-theory prediction

Ruijuan Xiao, Michael D. Kuz'min, Klaus Koepernik, and Manuel Richter

*IFW Dresden e.V., PO Box 270116, D-01171 Dresden,
Germany*

(Dated: 15 February 2022)

We report a density-functional study of the heteronuclear CoIr dimer adsorbed on benzene or graphene. In either case CoIr prefers an upright position above the center of a carbon hexagon with the Co atom next to it. The Ir atom stays away from the carbon ring and thus preserves its free-atom-like properties. This results in a very large magnetic anisotropy of more than 0.2 eV per dimer. So high a value should suffice for long-term data storage at the temperature of liquid nitrogen.

PACS numbers: 31.15.es, 75.30.Gw, 75.75.-c

Graphene has recently attracted much attention in both applied and fundamental science. Owing to its novel properties, graphene opens new perspectives for post-silicon electronics¹, spintronics², chemical sensor³, hydrogen storage⁴, touch-screen panel⁵, and further applications⁶. Recently, our density-functional-theory (DFT) investigations revealed that both benzene and graphene are suitable substrates to adsorb some transition-metal dimers (TMD) in a magnetic state of potential interest for high-density magnetic data storage^{7,8}. The hexagonal environment provided by the carbon ring preserves the electronic structure characteristics of the free Co dimer, which results in a magnetic anisotropy energy (MAE) of the order of 100 meV per dimer⁷. A systematic DFT study of a whole series of dimer-benzene complexes including the *3d* and *4d* TMD Fe₂, Co₂, Ni₂, Ru₂, Rh₂, and Pd₂ shows that promisingly large MAE, stable geometry, and stable magnetic ground state are also found in Ru₂Bz (Bz = C₆H₆).⁸ These findings may open a way to enhance the presently available area density of magnetic recording by up to three orders of magnitude. Considering that a minimum MAE of 40 *kT* is required for long-term data stability⁹, the reported^{7,8} MAE could be sufficient to operate a magnetic storage device at about 30 K. The aim of the present work is to seek a possibility to further raise the MAE of TMD complexes in order to extend the expected operation range to the temperature of liquid nitrogen.

Spin-orbit interaction in a magnetic state is the primary source of MAE¹⁰. Recent DFT calculations found that in the Co group, along with the increasing strength of the spin-orbit coupling parameter, the free dimer MAE increases from Co₂ to Ir₂.^{11–15} Thus, depositing *5d*-TMD like Ir₂, on Bz or on graphene (Gr) might be expected to result in a larger MAE of the dimer-carbon system than in the related *3d*-TMD case. Previous studies however tell us that chemical binding to surfaces frequently reduces the magnetic moment of *4d* or *5d* metals due to their relatively small intra-atomic exchange (Stoner) integrals¹⁶. For example, the calculated ground states of Rh₂ or Pd₂ adsorbed on Bz are non-magnetic.⁸ Heterodimers of *3d* and *5d* elements would combine a large Stoner integral (*3d*) with strong spin-orbit coupling (*5d*).

Electronic structure analysis suggests that only a perpendicular (upright) arrangement of the dimer on Bz or Gr (local symmetry *C*_{6v}) is helpful to preserve the large MAE of the dimer⁸. In such a configuration, Fig. 1 (a), the elemental identity of the atom next to the carbon ring determines the binding characteristics, while the atom atop contributes mostly to the magnetic properties of the system. Therefore, choosing light atoms as base atoms and

placing heavy atoms atop may be a way to utilize the stronger spin-orbit coupling in the latter without sacrificing the high magnetic moment. Here, we use the heteronuclear dimer CoIr to test this idea. The ground-state structures, binding energies, magnetic moments, and magnetic anisotropies of CoIr adsorbed on benzene and graphene were investigated. For comparison and deeper understanding, these properties were also studied in Ir₂Bz, in Co₂Bz, and in free CoIr, Ir₂, and Co₂ dimers.

Our DFT calculations were performed with a highly accurate all-electron full-potential local-orbital scheme (FPLO)¹⁷, release 9.00-34¹⁸. The molecular mode of FPLO with free boundary conditions and Fermi temperature broadening of 100 K was used for free dimer and dimer-Bz systems. To simulate the interaction between the dimer and Gr, a 4×4 supercell (space group P1) of dimension 9.84×9.84×16 Å³ was used, large enough to avoid interactions among dimers in neighboring cells. The related k-mesh used for linear-tetrahedron-method integrations contained 6×6×1 points in the Brillouin zone. All data reported here were obtained using the generalized gradient approximation (GGA) with the PBE96 exchange-correlation functional¹⁹. The valence basis set comprised Co (3*s*, 3*p*, 3*d*, 4*s*, 4*p*, 4*d*, 5*s*), Ir (4*f*, 5*s*, 5*p*, 5*d*, 6*s*, 6*p*, 6*d*, 7*s*), C (1*s*, 2*s*, 2*p*, 3*s*, 3*p*, 3*d*), and H (1*s*, 2*s*, 2*p*) states. Geometry optimization was carried out in a scalar relativistic mode with a force convergence threshold of 10⁻² eV/Å .

To find the lowest-energy geometries and spin states of the CoIrBz complex, 18 kinds of initial structures were optimized without any symmetry constraints for total spin $S = 0, 1, 2$, and 3. (See Fig. A1(i)-(vi) and (ix)-(xiv) of Ref. 8. The structures (vii) and (viii) were ignored since there the distance between metal atoms is too short to be reasonable. For structures (i), (vi), (ix), (xi), (xii), and (xiii), 6 new variants appear by interchanging the positions of Co and Ir atoms.) Initial antiferromagnetic and ferrimagnetic states were also considered for $S = 0$ and 1.

For CoIrGr, 9 initial configurations were considered, denoted by \parallel_{cc} , \parallel_{mm} , \parallel_{tt} , \perp_{cCoIr} , \perp_{cIrCo} , \perp_{mCoIr} , \perp_{mIrCo} , \perp_{tCoIr} and \perp_{tIrCo} . Here, \perp or \parallel mean that the dimer axis is oriented perpendicular or parallel to the Gr plane, respectively; c, m, and t denote that Co and Ir are placed above the center of a carbon ring, above the midpoint of a C-C bond, or on top of a C atom, respectively. In the \perp configurations, the atom mentioned first is next to the Gr plane. All carbon positions were fixed in the plane with a C-C bond length of 1.42 Å.

The MAE of CoIrBz or CoIrGr in the ground state was computed as the energy difference,

$E^{[100]} - E^{[001]}$, between states with magnetization direction perpendicular $[0\ 0\ 1]$ and parallel $[1\ 0\ 0]$ to the carbon plane. The in-plane anisotropy was neglected, $[1\ 0\ 0]$ was defined to point from the center to the corner of the carbon hexagon. In the case of free dimers, $[0\ 0\ 1]$ and $[1\ 0\ 0]$ stand for the directions parallel and perpendicular to the dimer axis. The MAE was evaluated in the fully relativistic mode in which spin-orbit coupling is included in all orders. As a matter of experience⁷, the MAE values obtained within standard GGA and by including the orbital polarization correction²⁰ give respectively a lower and an upper estimate of the expected MAE.

Benzene is a good model system to describe the main characteristics of dimer adsorption on graphene^{7,21}. In Fig. 1 we present the ground state and the four lowest-energy isomers of the CoIrBz complex, obtained by the described optimization. In the ground state, the CoIr dimer is bound perpendicularly to benzene with Co next to the carbon ring (C_{6v} symmetry, Fig. 1(a)). The distance between Co and Ir in the free dimer is 2.13 Å. This metal-metal bond length is increased by only 3% in the cases of upright adsorption (Fig. 1(a), (d)), while it is enlarged by about 10% in the parallel adsorption modes (Fig. 1(b), (c), (e)). The dimer adsorption energy, E_{ad} , in the ground state is 1.51 eV, which is comparable to the E_{ad} value of Co₂Bz, 1.47 eV (Tab. I). We also notice that the calculated E_{ad} of Ir₂Bz, 1.74 eV, is larger than that of Co₂Bz or CoIrBz. For an upright adsorption with Ir next to Bz (not shown in Fig. 1), we found a ferrimagnetic state with $E_{ad} = 0.94$ eV and $S = 1$ at almost the same energy as a ferromagnetic state with $S=2$.

A detailed understanding of adhesion and isomer energies is complex and beyond the scope of this paper. It would require consideration of the transition-metal level positions in different spin states, their different orbital overlap and their element-specific Stoner integrals. To give just one example, we note that the Co contribution to the bonding π -states of CoIrBz situated at about -8 eV (Fig. 2) is quite different in the two spin channels. This originates from the spin-splitting of the CoIr- π states, right-hand panel of Fig. 2, and the resulting unequal energy differences from the Bz-HOMO level.

The ground-state spin of CoIrBz, $S = 2$, equals that of the free CoIr-dimer. This makes a welcome difference to Ir₂, whose moment is completely quenched when it is adsorbed by benzene. Using the heteronuclear dimer CoIr instead of Ir₂ protects the magnetism of the heavy atom since it stays atop and preserves its free-atom-like properties to a large extent. In the ground state of the CoIrBz complex, the magnetic moments of Co and Ir are about

1.8 μ_B and 2.3 μ_B , respectively. Compared with the free CoIr dimer, the magnetic moment of Co decreases while that of Ir increases (Tab. I). Fig. 2 shows the energy level scheme and the orbital composition of each level for the ground states of CoIrBz and of CoIr. Like in Co₂Bz,⁸ the adsorption is realized mainly by forming chemical bonds between carbon and the atom next to the benzene plane. For example, the $3d_{xy}$, $3d_{x^2-y^2}$ orbitals of the Co atom and the LUMO of benzene form the δ states at -5.9 eV/-1.7 eV (majority spin channel) and -4.8 eV/-1.5 eV (minority spin channel). The π states around -8 eV in both spin channels mainly consist of the $3d_{xz}$, $3d_{yz}$ orbitals of Co and the HOMO of benzene. At the Fermi level, a two-fold degenerate singly occupied δ^* state is to 90% composed of the $5d_{xy}$, $5d_{x^2-y^2}$ states of Ir. It is the splitting of this state by the spin-orbit interaction that determines the MAE of the whole system.

The value of MAE and the site-resolved spin and orbital moments μ_S and μ_L for both magnetization orientations are listed in Tab. II. Data for free CoIr and for CoIrGr (discussed below) are included for comparison. In all systems, the spin moments are nearly the same for [0 0 1] and for [1 0 0] orientation, but the anisotropy of the orbital moments is obvious. The Ir atom shows large orbital moments in the case of [0 0 1] orientation and relatively small values in the [1 0 0] case. The Co atoms behave differently in the free and in the bound dimers. In free CoIr, the orbital moment of Co in the [0 0 1] orientation is around 0.9 μ_B , much larger than in the [1 0 0] orientation. When bound to benzene, the orbital moment of Co is quenched. This comes about through a re-distribution of Co-weight between the δ and δ^* states in the minority spin channel, see Fig. 2. Interaction with Bz leads to a severe reduction of Co-weight in δ^* in favor of the $\delta(\delta)$ and $\pi^*(\delta)$ states. As a result, the singly occupied δ^* molecular orbital, carrying a large ground-state orbital moment of nearly 2 μ_B , is situated almost exclusively on the Ir atom.

The calculated lower and upper estimates of the MAE in CoIrBz are about 250 meV and 290 meV, respectively. Both of them are larger than either of the values for free CoIr. The reason is that the MAE is proportional to the orbital moment anisotropy and grows with the strength of spin-orbit coupling⁸ and that bonding to benzene results in a significant increase of the former on the Ir atom (Tab. II).

Most notably, the *lower* estimate of the MAE of CoIrBz is *five times* higher than the respective estimate for Co₂Bz.⁷ Because the spin-orbit coupling in Ir is much stronger than in Co, the MAE caused by the Ir orbital moment anisotropy in CoIrBz is correspondingly

much larger than the purely Co-related MAE in Co₂Bz. We also notice that Co₂Bz has a slightly higher upper MAE estimate than CoIrBz, which is due to⁸ the larger Racah parameter B of Co (145 meV) than of Ir (94 meV).

Finally, we investigated the properties of a CoIr dimer deposited on graphene. Structural optimizations of all 9 initial configurations confirm that the CoIr dimer is adsorbed by Gr in an upright position with local symmetry C_{6v} , and that the Co atom prefers to occupy the position next to the Gr plane. The calculated dimer adsorption energy for the ground state amounts to 0.63 eV, and the relative energy of two separate adatoms to a bound dimer, $[E_{\text{CoGr}} + E_{\text{IrGr}} - E_{\text{Gr}}] - E_{\text{CoIrGr}}$, is 3.34 eV. This clearly indicates that the metal atoms prefer to aggregate as dimers rather than as separate adatoms. The Co-Ir bond length and the Co-C bond length are 2.18 Å and 2.25 Å, respectively, similar to the CoIrBz case. A band-structure analysis (not shown) for the ground state geometry and spin of CoIrGr indicates that the main contribution to the states near the Fermi level originates from the $5d_{x^2-y^2}$ and $5d_{xy}$ orbitals of Ir. Like in CoIrBz, the Ir atom in CoIrGr shows free-atom-like properties and its orbital moment anisotropy gives rise to a very large MAE estimated to be between 200 meV and 330 meV.

In summary, the CoIr hetero-dimer is expected to bind with benzene/graphene in perpendicular orientation above the center of a carbon hexagon with the Ir atom farther away from carbon than the Co atom. Due to its remote position, the Ir atom largely preserves its free-atom-like properties. We predict that this kind of binding does not result in a deterioration of the magnetic moment of the CoIr dimer and that the MAE of this structure amounts to 0.2 ... 0.3 eV. These numbers exceed all known experimental values of MAE by more than one order of magnitude. Judging by the criterion $\text{MAE} > 40 kT$,⁹ CoIrGr should be a promising material for ultrahigh-density magnetic data storage at liquid-nitrogen temperature. The demonstrated similarity of our results for CoIrBz and CoIrGr suggests a possibility to use other substrates, like boron-nitride or various aromatic carbon-hydrates, with a related chance to achieve chemical self-assembling.

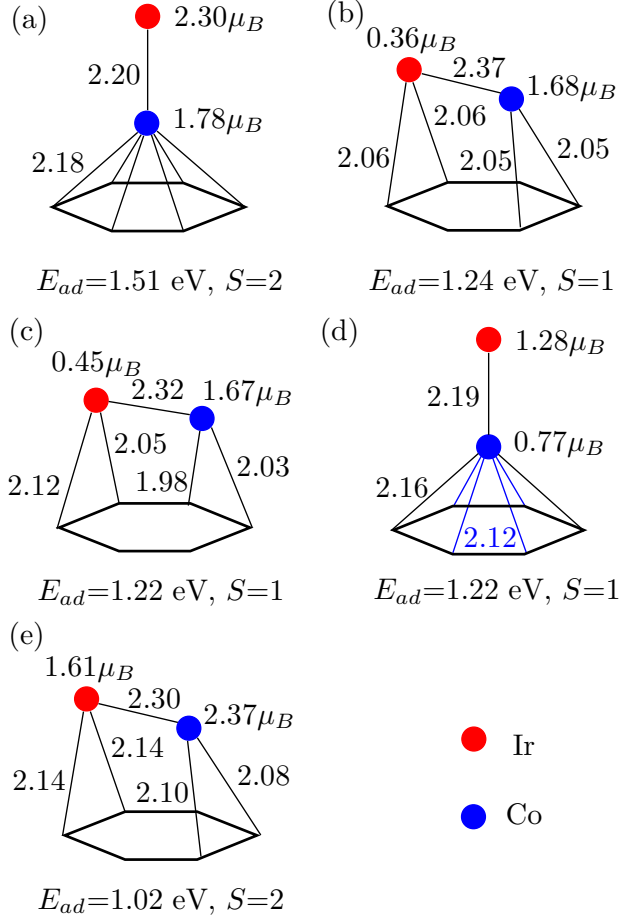


FIG. 1. (Color online) The dimer adsorption energy (E_{ad}), metal-metal and metal-carbon bond lengths (in Å), and spin magnetic moments for the ground-state geometry (a) and higher energy geometries or spin states (b)-(e) of the CoIrBz complex. Hexagons indicate benzene rings. The red and blue bullets indicate Ir and Co atoms, respectively.

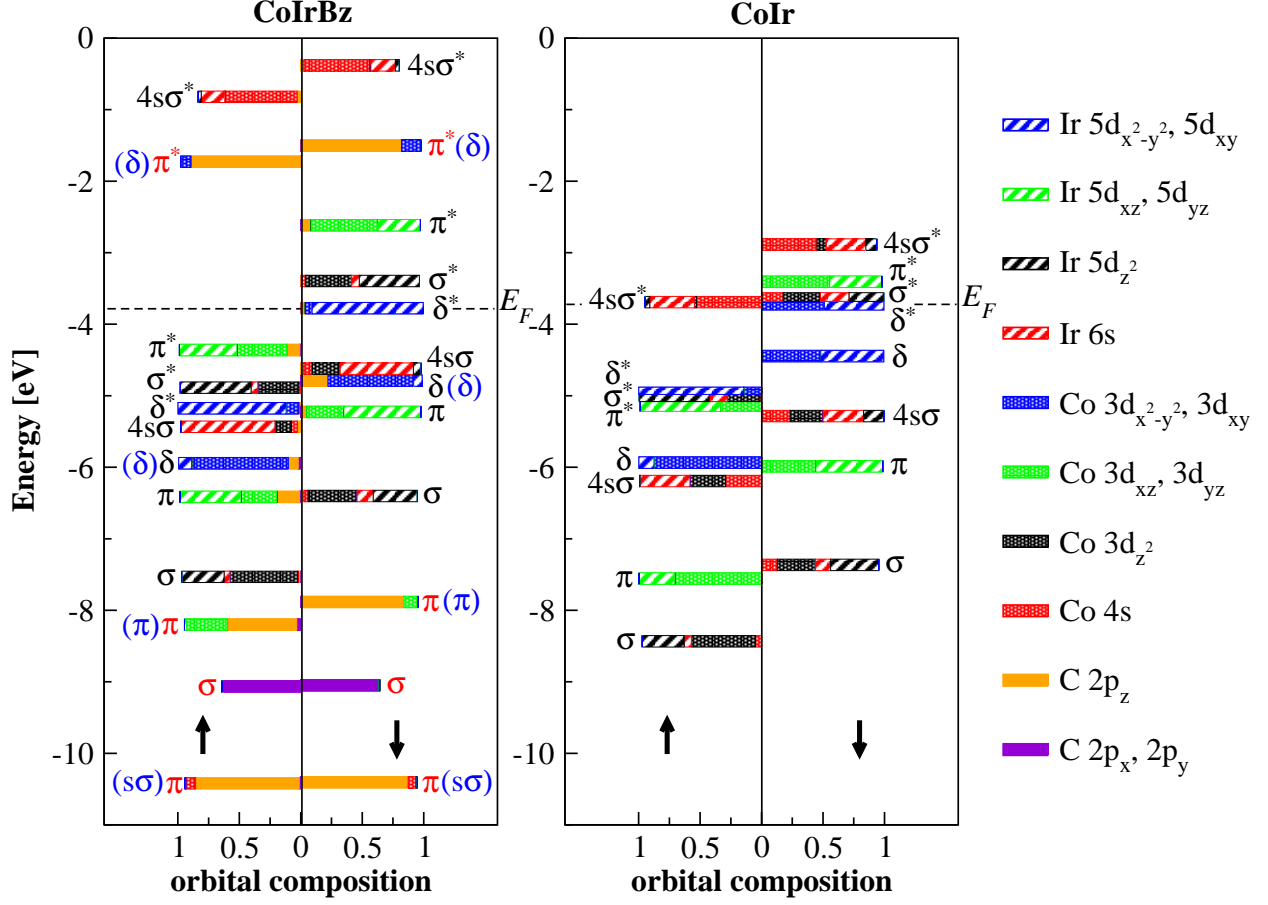


FIG. 2. (Color online) Scalar-relativistic single-particle energy levels and their orbital compositions for the ground states of CoIrBz (left panel) and CoIr (right panel). The upward (downward) arrow indicates majority (minority) spin states. All energies refer to a common vacuum level. Dimer-dominated states are labelled in black and benzene-dominated states are labelled in red. The three types of chemical bonds between the CoIr dimer and Bz are labelled blue in parentheses. The position of the Fermi level (E_F) is indicated by a horizontal dashed line. For better resolution, the δ^*_\uparrow -level of CoIr is raised by 0.160 eV, the σ^*_\uparrow -level is raised by 0.005 eV, and the π^*_\uparrow -level is lowered by 0.012 eV.

TABLE I. Dimer adsorption energy E_{ad} , total spin S , atom-resolved spin magnetic moments, $\mu_{S(\text{TM1})}$ and $\mu_{S(\text{TM2})}$, metal-metal and metal-carbon bond lengths, $d_{\text{TM1-TM2}}$ and $d_{\text{TM1-C}}$, for the ground state of Co_2 , Co_2Bz , Ir_2 , Ir_2Bz , CoIr , CoIrBz , and CoIrGr . TM1 denotes the atom next to the carbon plane and TM2 the atom farther away. The data for Co_2Bz differ slightly from our previous results⁷, because in this work full structural optimization was performed, while in Ref. 7 the Bz plane was fixed.

system	Co_2	Co_2Bz	Ir_2	Ir_2Bz	CoIr	CoIrBz	CoIrGr
E_{ad} (eV)	—	1.47	—	1.74	—	1.51	0.63
S	2	2	2	0	2	2	2
$\mu_{S(\text{TM1})}$ (μ_B)	2.00	1.63	2.00	0.00	2.08	1.78	1.81
$\mu_{S(\text{TM2})}$ (μ_B)	2.00	2.46	2.00	0.00	1.92	2.30	2.28
$d_{\text{TM1-TM2}}$ (\AA)	2.00	2.09	2.26	2.25	2.13	2.20	2.18
$d_{\text{TM1-C}}$ (\AA)	—	2.16	—	2.28	—	2.18	2.25

TABLE II. Spin and orbital moments μ_S and μ_L (in μ_B) and MAE ($E_{tot}^{[100]} - E_{tot}^{[001]}$, in meV) of the ground states of CoIr, CoIrBz and CoIrGr. Values calculated with and without the OP correction are given in the columns entitled SO+OP and SO, respectively.

	CoIr		CoIrBz		CoIrGr	
	SO	SO+OP	SO	SO+OP	SO	SO+OP
$\mu_{S(\text{Co})}^{[001]}$	2.05	2.05	1.74	1.73	1.74	1.73
$\mu_{S(\text{Co})}^{[100]}$	2.14	2.15	1.73	1.74	1.82	1.82
$\mu_{L(\text{Co})}^{[001]}$	0.89	0.95	0.06	-0.04	0.09	-0.05
$\mu_{L(\text{Co})}^{[100]}$	0.14	0.60	0.23	0.48	0.28	0.65
$\mu_{S(\text{Ir})}^{[001]}$	1.84	1.82	2.20	2.21	2.17	2.20
$\mu_{S(\text{Ir})}^{[100]}$	1.80	1.84	2.01	2.06	2.04	2.07
$\mu_{L(\text{Ir})}^{[001]}$	1.26	1.23	2.02	2.13	1.83	2.03
$\mu_{L(\text{Ir})}^{[100]}$	0.66	0.96	0.62	0.81	0.63	0.99
$\mu_{L(\text{total})}^{[001]}$	2.15	2.18	2.08	2.09	1.92	1.98
$\mu_{L(\text{total})}^{[100]}$	0.80	1.56	0.85	1.29	0.91	1.64
MAE	142	230	248	289	198	327

REFERENCES

- ¹A. K. Geim and K. S. Novoselov, *Nature Mater.*, **6**, 183 (2007).
- ²V. M. Karpan, G. Giovannetti, P. A. Khomyakov, M. Talanana, A. A. Starikov, M. Zwierzycki, J. van den Brink, G. Brocks, and P. J. Kelly, *Phys. Rev. Lett.*, **99**, 176602 (2007).
- ³F. Schedin, A. K. Geim, S. V. Morozov, E. W. Hill, P. Blake, M. I. Katsnelson, and K. S. Novoselov, *Nature Mater.*, **6**, 652 (2007).
- ⁴H. Lee, J. Ihm, M. L. Cohen, and S. G. Louie, *Nano Lett.*, **10**, 793 (2010).
- ⁵S. Bae, H. Kim, Y. Lee, X. Xu, J.-S. Park, Y. Zheng, J. Balakrishnan, T. Lei, H. R. Kim, Y. I. Song, Y.-J. Kim, K. S. Kim, B. Özyilmaz, J.-H. Ahn, B. H. Hong, and S. Iijima, *Nature Nanotech.*, **5**, 574 (2010).
- ⁶M. J. Allen, V. C. Tung, and R. B. Kaner, *Chem. Rev.*, **110**, 132 (2010).
- ⁷R. Xiao, D. Fritsch, M. D. Kuz'min, K. Koepernik, H. Eschrig, M. Richter, K. Vietze, and G. Seifert, *Phys. Rev. Lett.*, **103**, 187201 (2009).
- ⁸R. Xiao, D. Fritsch, M. D. Kuz'min, K. Koepernik, M. Richter, K. Vietze, and G. Seifert, (2010), arXiv:1009.0170v2.
- ⁹S. H. Charap, P.-L. Lu, and Y. He, *IEEE Trans. Magn.*, **33**, 978 (1997).
- ¹⁰H. Brooks, *Phys. Rev.*, **58**, 909 (1940).
- ¹¹T. O. Strandberg, C. M. Canali, and A. H. MacDonald, *Nature Mater.*, **6**, 648 (2007).
- ¹²T. O. Strandberg, C. M. Canali, and A. H. MacDonald, *Phys. Rev. B*, **77**, 174416 (2008).
- ¹³P. Błoński and J. Hafner, *Phys. Rev. B*, **79**, 224418 (2009).
- ¹⁴D. Fritsch, K. Koepernik, M. Richter, and H. Eschrig, *J. Comp. Chem.*, **29**, 2210 (2008).
- ¹⁵L. Fernández-Seivane and J. Ferrer, *Phys. Rev. Lett.*, **99**, 183401 (2007).
- ¹⁶I. Cabria, B. Nonas, R. Zeller, and P. H. Dederichs, *Phys. Rev. B*, **65**, 054414 (2002).
- ¹⁷K. Koepernik and H. Eschrig, *Phys. Rev. B*, **59**, 1743 (1999).
- ¹⁸<http://www.fplo.de>.
- ¹⁹J. P. Perdew, K. Burke, and M. Ernzerhof, *Phys. Rev. Lett.*, **77**, 3865 (1996).
- ²⁰O. Eriksson, M. S. S. Brooks, and B. Johansson, *Phys. Rev. B*, **41**, 7311 (1990).
- ²¹J. J. BelBruno, *Surf. Sci.*, **577**, 167 (2005).